Proceedings of the 2002 IEEE
International Conference on Robotics & Automation
Washington, DC • May 2002

Impulse Measure Based Performance Analysis of Sawing Task by Dual Arm

Jae Hoon Lee, Byung-Ju Yi, Sang-Rok Oh*, and Il Hong Suh

E-mail : bj@hanyang.ac.kr
School of Electrical Engineering and Computer Science, Hanyang University, KOREA
*Intelligent System Control Research Center, KIST, KOREA

Abstract *- Some of manufacturing tasks such as sawing task often requires continuous impulsive motion. In case of sawing task, such impulsive motions can be observed between the teeth of the saw and the object. The amount of the external impulse exerted on the object has been treated as an important control parameter. Also, the internal impulses experienced at the joints should be simultaneously taken into account to avoid serious damage or injury at the joints.*

The purpose of this work is to improve the efficacy of sawing task by using dual arm. For this, an external impulse model for sawing task is suggested. Also, the closed-form internal impulse models are proposed for both a single and dual arms. Based on these models, a new measure for internal impulse is proposed. A normalized impulse ellipsoid reflecting the velocity direction is employed to visualize the impact geometry. Finally, the optimal sawing region is identified in which the amount of external impulse is maximized and the amount of the internal impulse is minimized. It is demonstrated through simulation that the dual arm exhibits better sawing performance over a single arm in aspects of external and internal impulses.

I. INTRODUCTION

Fig. 1 shows the human sawing task. The external impulse acting on the object in manufacturing tasks is the function of the posture and the dynamic characteristic of the worker. In most of robot control problems dealing with impact, the robot is controlled to minimize the amount of external impulse transmitted to the robot upon abrupt contact. On the contrary, the amount of external impulse should be maximized in some manufacturing tasks. However, the internal impulse experienced at the joints of the human-body should be minimized to avoid injury or damage. For such purpose, human usually identifies how to saw and where to saw by experiences. But, the robot should be trained to perform the sawing task effectively.

Methods to evaluate the impulses occurring in general collisions have been proposed by several researchers [1-4, 6-12]. Walker investigated the external impulse model for serial-type manipulator and also proposed an impact measure for kinematically redundant and multiple armed robotic systems [1]. Liao and Leu [2] presented the Lagrangian external impact model to derive an impact equation for an industrial manipulator. Zheng and Hemami [3] derived the internal impulse model at the joints by using Newton-Euler equations, but their model was confined to the serial-type manipulators. Wittenburg provided a general methodology in an implicit form for modeling external and internal impulses [4].

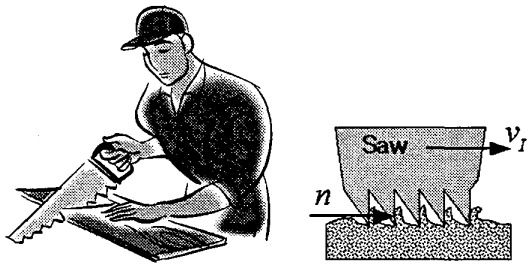

Fig. 1. Human Sawing Task

However, this model is not directly applicable to robotic systems. Kim, et al. [8] proposed a normalized impact geometry and performance measure based on velocity direction. However, their algorithm was confined to external impulse model for serial robotic system. Lee and Yi, et al. [9] proposed a closed-form, explicit external and internal impulse models for general classes of multi-body mechanisms.

Multiple cooperating robots can perform tasks more efficiently, which cannot be carried out by using a single arm. These tasks include the handling of heavy and large objects, and assembly of complex parts or part mating, and so on. One of the typical features of such multiple robot systems is redundant actuation mode. This mode enhances the performances of the system in aspects of singularity avoidance, increase of payload, stiffness, and development of multiple sub-criteria. In this work, we investigate the advantage of dual arms or multiple arms in the viewpoint of impulses.

II. DYNAMICS OF GENERAL ROBOT SYSTEM

To model general hybrid mechanism containing serial-chains as well as closed-chains, we convert the system as an open-tree structure shown in Fig. 2. The open-tree structure is made by cutting joints (or links) of the closed chains. First, the dynamic model of each serial-chain is evaluated. Then, the dynamic model in terms of the independent coordinates is given by [5]

$$\boldsymbol{T}_a = [\boldsymbol{I}^*_{aa}]\ddot{\boldsymbol{\phi}}_a + \dot{\boldsymbol{\phi}}_a^T[\boldsymbol{P}^*_{aaa}]\dot{\boldsymbol{\phi}}_a, \qquad (1)$$

where $\boldsymbol{T}_a$ denotes the inertial load vector referenced to the independent joint set. $[\boldsymbol{I}^*_{aa}]$ and $[\boldsymbol{P}^*_{aaa}]$ represent the inertia matrix and the inertia power array referenced to the independent joint set, respectively.

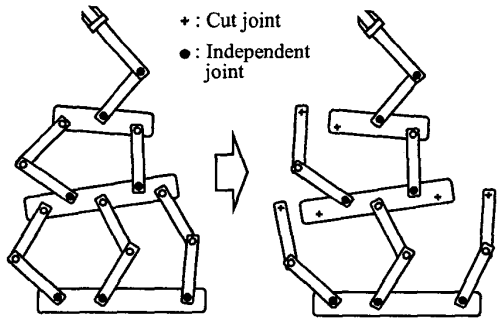

Fig. 2 Schematic diagram of open-tree structure

III. External Impulse Model for Sawing Task

Most generally, the impact is partially elastic in the range of $0 < e < 1$. When the coefficient of restitution e is known, the relative velocity of colliding bodies can be obtained immediately after the impact. The component of the increment of relative velocity along a vector $\boldsymbol{n}$ that is normal to the contact surface is given by [4]

$$(\Delta \upsilon_1 - \Delta \upsilon_2)^T \boldsymbol{n} = -(1+e)(\upsilon_1 - \upsilon_2)^T \boldsymbol{n}, \qquad (2)$$

where υ_1 and υ_2 are the absolute velocities of the colliding bodies immediately before impact, and $\Delta\upsilon_1$ and $\Delta\upsilon_2$ are the velocity increments immediately after impact.

When a robot system interacts with environment, the dynamic model of the robot referenced to the independent joint set is given by

$$\boldsymbol{T}_a = [\boldsymbol{I}^*_{aa}]\ddot{\phi}_a + \dot{\phi}_a{}^T[\boldsymbol{P}^*_{aaa}]\dot{\phi}_a - [\boldsymbol{G}^{\upsilon_I}_a]^T \boldsymbol{F}_I, \qquad (3)$$

where $\boldsymbol{F}_I$ is the impulsive external force at the contact point and $[\boldsymbol{G}^{\upsilon_I}_a] \in \Re^{3\times N_a}$ given in

$$\mathrm{u}_I = [\boldsymbol{G}^{\upsilon_I}_a]\dot{\phi}_a \qquad (4)$$

denotes the 1st order KIC relating the contact point's velocity u_I with respect to the inertial frame to the independent joint's velocity.

Integration of the dynamic model given in Eq. (3) over contacting time interval gives

$$\int_{t_0}^{t_0+\Delta t} \boldsymbol{T}_a dt = \int_{t_0}^{t_0+\Delta t} [\boldsymbol{I}^*_{aa}]\ddot{\phi}_a\, dt + \int_{t_0}^{t_0+\Delta t} \dot{\phi}_a^T [\boldsymbol{P}^*_{aaa}]\dot{\phi}_a dt - \int_{t_0}^{t_0+\Delta t} [\boldsymbol{G}^{\upsilon_I}_a]^T \boldsymbol{F}_I dt. \qquad (5)$$

Since the positions and velocities are finite at all times as Δt goes to zero, the integral term involving $\dot{\phi}_a{}^T[\boldsymbol{P}^*_{aaa}]\dot{\phi}_a$ becomes zero, as does that involving actuation input $\boldsymbol{T}_a$. Thus, we obtain the following simple expression [1]

$$[\boldsymbol{I}^*_{aa}]\big(\dot{\phi}(t_0+\Delta t) - \dot{\phi}(t_0)\big) = [\boldsymbol{G}^{\upsilon_I}_a]^T \tilde{\boldsymbol{F}}_I, \qquad (6)$$

where $\tilde{\boldsymbol{F}}_I = \int_{t_0}^{t_0+\Delta t} \boldsymbol{F}_I dt$ is defined as the external impulse at the contact point. From Eq. (6), the velocity increment of the joint variables is obtained as

$$\Delta\dot{\phi}_a = [\boldsymbol{I}^*_{aa}]^{-1}[\boldsymbol{G}^{\upsilon_I}_a]^T \tilde{\boldsymbol{F}}_I, \qquad (7)$$

and the velocity increment at the contact point is obtained by the following kinematic relationship.

$$\Delta \mathrm{u}_I = [\boldsymbol{G}^{\upsilon_I}_a]\Delta\dot{\phi}_a = [\boldsymbol{G}^{\upsilon_I}_a][\boldsymbol{I}^*_{aa}]^{-1}[\boldsymbol{G}^{\upsilon_I}_a]^T \tilde{\boldsymbol{F}}_I, \qquad (8)$$

Now, let us consider a sawing task. Fig. 3 shows a chip model in the sawing task. A sawing task can be considered as a continuous collision between the teeth of the saw and the chip to be fabricated, and the impulsive force due to collision creates fracture of the chip. We assume that the fracture happens due to the shearing moment formed at the bottom of the chip. Thus, the motion of the chip created by fracture can be simply modeled as a revolute joint.

Similar to (7), the velocity increment of the joint variable of the chip is

$$\Delta\dot{\gamma} = [\boldsymbol{I}^*_{\gamma C}]^{-1}[\boldsymbol{G}^C_\gamma]^T(-\tilde{\boldsymbol{F}}_I), \qquad (9)$$

where $[\boldsymbol{G}^C_\gamma]$ is the Jacobian that relates the velocity of the center of mass of the chip to the velocity vector of the joint of the chip model in Fig. 3, and $[\boldsymbol{I}^*_{\gamma C}]$ denotes the inertia matrix of the chip to be fabricated. Then, the velocity increment of the chip at the contact point is obtained by the following kinematic relationship

$$\Delta\upsilon_C = [\boldsymbol{G}^C_\gamma]\Delta\dot{\gamma} = [\boldsymbol{G}^C_\gamma][\boldsymbol{I}^*_{\gamma C}]^{-1}[\boldsymbol{G}^C_\gamma]^T(-\tilde{\boldsymbol{F}}_I). \qquad (10)$$

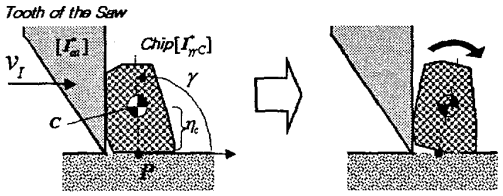

Fig. 3. Chip Model

Assume that the saw collides with the object to be sawn and that the chip is formed according to the model of Fig. 3. Substitution of Eq. (8) and Eq. (10) into Eq. (2) gives

$$\left\{\left([\boldsymbol{G}^{\upsilon_I}_a][\boldsymbol{I}^*_{aa}]^{-1}[\boldsymbol{G}^{\upsilon_I}_a]^T + [\boldsymbol{G}^C_\gamma][\boldsymbol{I}^*_{\gamma C}]^{-1}[\boldsymbol{G}^C_\gamma]^T\right)\tilde{\boldsymbol{F}}_I\right\}^T \boldsymbol{n} = -(1+e)(\upsilon_I - \upsilon_C)^T \boldsymbol{n} \qquad (11)$$

Then, from Eq. (11), the external impulse exerted on the chip by the saw can be evaluated as follows:

$$\tilde{\boldsymbol{F}}_I = \left(\frac{-(1+e)(\upsilon_I - \upsilon_C)^T \boldsymbol{n}}{\boldsymbol{n}^T\{[\boldsymbol{G}^{\upsilon_I}_a][\boldsymbol{I}^*_{aa}]^{-1}[\boldsymbol{G}^{\upsilon_I}_a]^T + [\boldsymbol{G}^C_\gamma][\boldsymbol{I}^*_{\gamma C}]^{-1}[\boldsymbol{G}^C_\gamma]^T\}\boldsymbol{n}}\right)\boldsymbol{n}, \qquad (12)$$

where $[\boldsymbol{I}^*_{aa}]$ denotes the inertia matrix of the human arm grasping a saw and $[\boldsymbol{G}^{\upsilon_I}_a]$ represents the Jacobian of the contact point referenced to the joint input variables of the robot. It is noted that the external impulse is the function of robot configuration and the dynamic parameters of the sawing

task.

The value of e is 0 for purely plastic collisions (the colliding bodies have zero relative velocity to each other at the point of contact immediately following collision) and 1 for purely elastic collisions. Values of e between 0 to 1 indicate intermediate cases of the above two.

For the situation of a robot arm in contact with a solid object, such as a wall, we have the condition, $\upsilon_C = \Delta\upsilon_C = 0$. And the external impulse $\hat{F}_I$ is derived as

$$\tilde{F}_I = \left(\frac{-(1+e)(\upsilon_I)^T n}{n^T \left([G_a^{\upsilon_I}][I_{aa}^*]^{-1}[G_a^{\upsilon_I}]^T \right) n} \right) n. \tag{13}$$

In the sawing task, the object to be sawn is initially stationary and the sawn chip deforms permanently. Thus, we have $\upsilon_C = 0$ and $e = 0$. The external impulse $\hat{F}_I$ for sawing task is then given by

$$\tilde{F}_I = \left(\frac{-(\upsilon_I)^T n}{n^T \{ [G_a^{\upsilon_I}][I_{aa}^*]^{-1}[G_a^{\upsilon_I}]^T + [G_\gamma^C][I_{\gamma\gamma C}^*]^{-1}[G_\gamma^C]^T \} n} \right) n, \tag{14}$$

where the first term and the second term of the denominator represents the effective dynamics contributing to the impulsive force. The first term is associated with the manipulator dynamics. In the meanwhile, the second term is associated with the fracture geometry and the material property of the chip to be sawn. Usually, the hardness of the object to be sawn changes magnitude of the external impulse. Thus, much bigger impulsive force would be required to remove the harder material as compared to soft material. The second term explains this phenomenon.

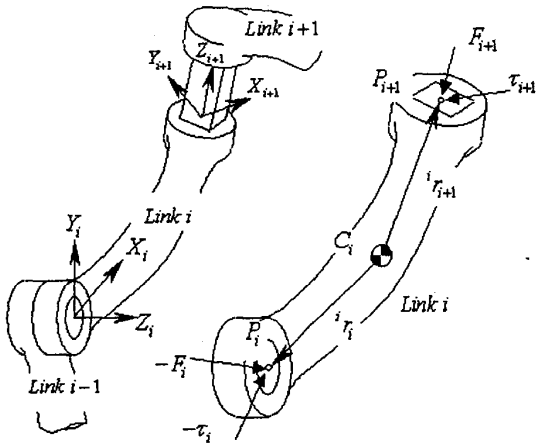

Fig. 4. Link and Joint System of Serial-chain

IV. Internal Impulse Modeling for Serial Chain

When a robot collides with environment, not only contact point but also all the joints experience impact. These impulses at the joint are called as *internal impulses*, Joint constrains the motions of the links to keep two links always connected. The motion degree-of-freedom of the joint determines the constraints. To constrain the motion, constraint forces and moments act at each joint. For example, in the case of revolute joint, three constraint forces and two constraint moments are exerted. The impulses are exerted along these constraint directions when the system collides with environment.

Excessive impulse may cause deformation or damage of the joint, because impact applies large force intensively for very short time interval in contrast to static load. Thus, the internal impulses at the joints have to be considered profoundly, and the method to evaluate the internal impulses is introduced here.

First, the external impulse and the velocity increments at the contact point and the joints are assumed known. Then, the internal impulses at the joints are evaluated as follows. Consider one body of a serial-chain system shown in Fig. 4. P_i is the absolute position vector of the point of ith body in contact with (i-1)th body, and ${}^i r_i$ is the position vector directing from the mass center C_i of link i to the contact point P_i.

The contact point is assumed as the center of the joint. F_i and τ_i are the impulsive force and the impulsive moment at the ith contact point, respectively. These impulsive forces and moments between interacting bodies are equal in magnitude, opposite in direction and collinear. Based on Newton-Euler's equation, the dynamics of the ith body with respect to ith coordinate frame can be obtained as

$$m_i {}^i\upsilon_{C_i} = -{}^iF_i + [{}_{i+1}^iR]^{i+1}F_{i+1} + {}^if \tag{15}$$

$$\begin{aligned}[{}^{C_i}I]{}^i\dot{\omega}_i + {}^i\omega_i \times [{}^{C_i}I]{}^i\omega_i &= -{}^i\tau_i + [{}_{i+1}^iR]^{i+1}\tau_{i+1} \\ &\quad -{}^ir_i \times {}^iF_i + {}^ir_{i+1} \times [{}_{i+1}^iR]^{i+1}F_{i+1} + {}^i\tau\end{aligned}, \tag{16}$$

where m_i and $[{}^{C_i}I]$ are the mass and the moment of inertia of the ith body, respectively. The velocity of the mass center and angular velocity is noted as ${}^i\upsilon_{C_i}$ and ${}^i\omega_i$, respectively. The superscript in front of variable means the coordinate frame in which the variable is represented. ${}^if$ and ${}^i\tau$ represent the non-impulsive forces and moments acting on link i. $[{}_{i+1}^iR]$ is the rotation matrix transforming the (i+1)th coordinate system to ith coordinate system. By integrating the dynamics with respect to time, the relationships between the velocity increments and the impulses ($\tilde{F}$ and $\tilde{\tau}$) in the ith coordinate frame are obtained as

$$m_i \Delta {}^i\upsilon_{C_i} = -{}^i\tilde{F}_i + [{}_{i+1}^iR]^{i+1}\tilde{F}_{i+1}, \tag{17}$$

$$\begin{aligned}[{}^{C_i}I]\Delta {}^i\omega_i &= -{}^i\tilde{\tau}_i + [{}_{i+1}^iR]^{i+1}\tilde{\tau}_{i+1} \\ &\quad -{}^ir_i \times {}^i\tilde{F}_i + {}^ir_{i+1} \times [{}_{i+1}^iR]^{i+1}\tilde{F}_{i+1}\end{aligned}. \tag{18}$$

Consequently, the internal impulses at the joints of serial-chain systems are formulated as [9]

$$\begin{pmatrix}\tilde{F}\\ \tilde{\tau}\end{pmatrix}=[S_e^i]\begin{pmatrix}\tilde{F}_I\\ \tilde{\tau}_I\end{pmatrix}, \tag{19}$$

where $\tilde{F}=\left({}^1\tilde{F}_1^T,\cdots,{}^N\tilde{F}_N^T\right)^T$ and $\tilde{\tau}=\left({}^1\tilde{\tau}_1^T,\cdots,{}^N\tilde{\tau}_N^T\right)^T$.

V. Internal Impulse Modeling for Closed-Chain

The method to evaluate the internal impulses of closed-chain mechanism is introduced in this section [9]. First, the closed-chain system has to be transformed into an open-tree structure to evaluate the internal impulses at joints. A dual arm modeled as a planar six-bar mechanism is considered here to explain the modeling method because it is one of the simplest closed-chain systems. Cutting one joint as shown in Fig. 5 makes the open-tree structure of the six-bar mechanism. The cut joint need not necessarily be a particular joint, and any joint can be cut. Selection of the cut joint is very subjective to the modeler. However, cutting any other joint gives the same result.

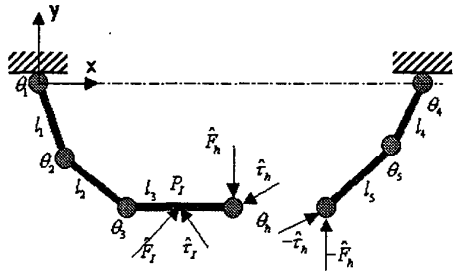

Fig. 5. Open-Tree Structure of the 6-bar Mechanism

In the figure, the cut joint is noted as ϕ_h. The impulse $\tilde{F}_h$ and the impulse moment $\tilde{\tau}_h$ at the cut joint act on the two serial-chains along opposite direction with the same magnitude. The point P_I contacting with environment is located in the left serial-chain. Then, the dynamic model of the left serial-chain is

$$\begin{aligned}{}_1\boldsymbol{T}=&[{}_1\boldsymbol{I}_{\phi\phi}^*]{}_1\ddot{\boldsymbol{\phi}}+{}_1\dot{\boldsymbol{\phi}}^T[{}_1\boldsymbol{P}_{\phi\phi\phi}^*]{}_1\dot{\boldsymbol{\phi}}\\&-[{}_1\boldsymbol{G}_\phi^h]^T\left(\boldsymbol{F}_h^T,\boldsymbol{\tau}_h^T\right)^T-[{}_1\boldsymbol{G}_\phi^I]^T\left(\boldsymbol{F}_I^T,\boldsymbol{\tau}_I^T\right)^T.\end{aligned} \tag{20}$$

The six-bar mechanism is assumed as a part of a complex hybrid mechanism in this procedure, so the external impulse moment can be considered as an impulse moment from another subsystem. $[{}_1G_\phi^I]$ is the 1st order KIC relating υ_I and ω_I to the joint velocity ${}_1\dot{\phi}$ of the left serial-chain. Thus, we have

$$\begin{pmatrix}\upsilon_I\\ \omega_I\end{pmatrix}=\begin{bmatrix}[{}_1G_\phi^{\upsilon_I}]\\ [{}_1G_\phi^{\omega_I}]\end{bmatrix}{}_1\dot{\phi}=[{}_1G_\phi^I]{}_1\dot{\phi}, \tag{21}$$

where $[{}_1G_\phi^h]$ denotes the 1st order KIC that relates the velocity υ_h of the cut joint to the joint velocity ${}_1\dot{\phi}$, and $[{}_1G_\phi^{\omega_{h1}}]$ relates the angular velocity ω_{h1} of the link 3 in contact with ϕ_h to the joint velocity ${}_1\dot{\phi}$. And the dynamic model of the right serial-chain is

$$\begin{aligned}{}_2\boldsymbol{T}=&[{}_2\boldsymbol{I}_{\phi\phi}^*]{}_2\ddot{\boldsymbol{\phi}}+{}_2\dot{\boldsymbol{\phi}}^T[{}_2\boldsymbol{P}_{\phi\phi\phi}^*]{}_2\dot{\boldsymbol{\phi}}\\&-[{}_2\boldsymbol{G}_\phi^h]^T\left(-\boldsymbol{F}_h^T,-\boldsymbol{\tau}_h^T\right)^T.\end{aligned} \tag{22}$$

Integration of Eqs. (20) and (22) over the time interval Δt gives following equations representing the relationship between the internal impulses and the velocity increments ;

$$\begin{aligned}\begin{pmatrix}\Delta\upsilon_h\\ \Delta\omega_{h1}\end{pmatrix}=&[{}_1G_\phi^h][{}_1I_{\phi\phi}^*]^{-1}[{}_1G_\phi^h]^T\begin{pmatrix}\tilde{F}_h\\ \tilde{\tau}_h\end{pmatrix},\\&+[{}_1G_\phi^h][{}_1I_{\phi\phi}^*]^{-1}[{}_1G_\phi^I]^T\begin{pmatrix}\tilde{F}_I\\ \tilde{\tau}_I\end{pmatrix}\end{aligned} \tag{23}$$

$$\begin{pmatrix}\Delta\upsilon_h\\ \Delta\omega_{h2}\end{pmatrix}=[{}_2G_\phi^h][{}_2I_{\phi\phi}^*]^{-1}[{}_2G_\phi^h]^T\begin{pmatrix}-\tilde{F}_h\\ -\tilde{\tau}_h\end{pmatrix}. \tag{24}$$

By rearranging the rows of Eqs. (23) and (24), we have the following matrix form, because the velocity increments are obtainable from $\tilde{F}_I$ and $\tilde{\tau}_I$.

$$[\boldsymbol{D}_h]\begin{pmatrix}\tilde{F}_I\\ \tilde{\tau}_I\end{pmatrix}=[\boldsymbol{A}_h]\begin{pmatrix}\tilde{F}_h\\ \tilde{\tau}_h\end{pmatrix}+[\boldsymbol{B}_h]\begin{pmatrix}\tilde{F}_I\\ \tilde{\tau}_I\end{pmatrix} \tag{25}$$

Thus $\tilde{F}_h$ and $\tilde{\tau}_h$ can be obtained in a closed form as

$$\begin{pmatrix}\tilde{F}_h\\ \tilde{\tau}_h\end{pmatrix}=[\boldsymbol{S}_e^h]\begin{pmatrix}\tilde{F}_I\\ \tilde{\tau}_I\end{pmatrix}. \tag{26}$$

where $[\boldsymbol{S}_e^h]=[\boldsymbol{A}_h]^{-1}([\boldsymbol{D}_h]-[\boldsymbol{B}_h])$ denotes the mapping matrix relating the external impulse to impulse at the cut joint.

Next, based on the impulse at the cut joints, the internal impulses of the two serial chains are evaluated as

$${}_1\tilde{F}=[{}_1\boldsymbol{S}_h^i][\boldsymbol{S}_e^h]\tilde{F}_I+[{}_1\boldsymbol{S}_e^i]\tilde{F}_I, \tag{27}$$

$${}_2\tilde{F}=[{}_2\boldsymbol{S}_h^i][\boldsymbol{S}_e^h]\tilde{F}_I, \tag{28}$$

where $[{}_j\boldsymbol{S}_h^i]$ and $[{}_j\boldsymbol{S}_e^i]$ are the mapping matrices of the j-th chain relating the external impulse at the cut joint to internal impulse and the mapping matrix relating the external impulse to internal impulses, respectively.

Finally, a closed form internal impulse model for a dual arm is obtained, by combining Eqs. (27) and (28), as

$$\begin{aligned}\tilde{F}_{\text{int}}=&\begin{bmatrix}[{}_1\boldsymbol{S}_h^I]\\ [{}_2\boldsymbol{S}_h^I]\end{bmatrix}[\boldsymbol{S}_e^h]\tilde{F}_I+\begin{bmatrix}[{}_1\boldsymbol{S}_e^I]\\ [0]\end{bmatrix}\tilde{F}_I,\\=&[\boldsymbol{S}_E^I]\tilde{F}_I\end{aligned} \tag{29}$$

where

$$\tilde{F}_{\text{int}}=\begin{pmatrix}{}_1\tilde{F}\\ {}_2\tilde{F}\end{pmatrix}. \tag{30}$$

VI. Impulse Geometry and Measure

Many former researchers developed various impulse geometries and impulse measures to evaluate the ability to withstand external impulse. However, measure and geometry for internal impulse has not been considered yet. In this chapter, we introduce various external impulse measures and impulse geometries along with suggestion of new internal impulse measure and geometry.

A. External impulse ellipsoid and external impulse measure

Walker [1] proposed *external (dynamic) impulse ellipsoid*, which represents relative magnitudes of the external impulsive forces corresponding to the unit ball of changes in joint velocities of the robot. Based on Eq. (7), the dynamic impulse ellipsoid in $\Re^m$ is described as

$$(\tilde{F}_I \in \Re^m : \tilde{F}_I^T [G_\phi^{\upsilon_I}][I_{\phi\phi}^*]^{-2}[G_\phi^{\upsilon_I}]^T \tilde{F}_I \le 1). \quad (31)$$

From Eq. (7), the dynamic impulse ellipsoid is formed by those contact impulse forces $\tilde{F}_I$ that correspond to changes in joint velocities $\Delta\dot{\phi}$ with unit norm or less, i.e., $\|\Delta\dot{\phi}\|^2 = \Delta\dot{\phi}^T \Delta\dot{\phi} \le 1$.

However, this method does not consider the magnitude and direction of the velocity, which plays an important role in the magnitude of the external impulse. And also the magnitude of this ellipsoid does not directly represent the impact force.

Kim, et al. [8] proposed a *normalized impact geometry* for serial manipulators. Consider Fig. 5 in which let $\boldsymbol{n}$ be the unit normal vector to the environment and $\boldsymbol{v}_I$ is the pre-impulse velocity to the normal direction of the object to be fabricated. *Normalized impulse geometry* in $\Re^m$ based on $\boldsymbol{n}^T\boldsymbol{v}_I$ is defined by

$$\left|\boldsymbol{n}^T \upsilon_I\right| \le 1. \quad (32)$$

Then,

$$\boldsymbol{n}^T([G_\phi^{\upsilon_I}][I_{\phi\phi}^*]^{-1}[G_\phi^{\upsilon_I}]^T)\boldsymbol{n}\frac{F_{imp}}{1+e} \le 1. \ (\boldsymbol{n} \in \Re^m) \quad (33)$$

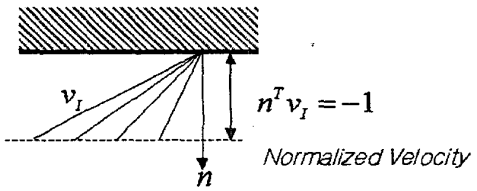

Fig. 6. Normalized Task Velocity

This means the range of directional impact force for given n-directional task velocity like Eq. (32). The magnitude and direction of task velocity, which play an important role in the magnitude of impulsive force, are considered in this geometry.

The normalized impact geometry can be extended to parallel manipulators. It is defined by

$$\boldsymbol{n}^T([G_a^{\upsilon_I}][I_{aa}^*]^{-1}[G_a^{\upsilon_I}]^T)\boldsymbol{n}\frac{F_{imp}}{1+e} \le 1, \ (\boldsymbol{n} \in \Re^m) \quad (34)$$

where $[I_{aa}^*]$ represent the inertia matrix referenced to the independent joint set, and $[G_a^{\upsilon_I}] \in \Re^{3\times N_a}$ is the 1st order KIC relating the contact point's velocity υ_I to the independent joint's velocity, respectively.

The normalized impact geometry is obtained from Eq. (34) by calculating the maximum value of F_{imp} for each direction of $\boldsymbol{n}$. The resulting ellipsoid is a form of belted ellipsoid.

From Eq. (12), we define the external impulse measure. In case of the sawing task, the velocity vector of the saw has the same direction as $\boldsymbol{n}$. That is, $\upsilon_I = |\upsilon_I|\boldsymbol{n}$ (refer to Fig. 1). Also note that e becomes zero in the manufacturing tasks yielding plastic deformation of the part to be fabricated. Thus, the external impulse measure for the sawing task is defined as

$$F_{imp} = \frac{-|\upsilon_I|}{\boldsymbol{n}^T\{[G_a^{\upsilon_I}][I_{aa}^*]^{-1}[G_a^{\upsilon_I}]^T + [G_\gamma^C][I_{\gamma\gamma C}^*]^{-1}[G_\gamma^C]^T\}\boldsymbol{n}}, \quad (35)$$

where F_{imp} is the magnitude of normalized external impulse.

B. Internal Impulse geometry and internal impulse measure

Previous research works only treated the impact geometry for external impulse. In this paper, we suggest a new internal geometry. The closed-form model of internal impulse given by Eq. (19) and Eq. (29) provides this function. The internal impulses of serial and closed-chain manipulators for a given external impulse are evaluated by

$$\tilde{F}_{int} = [S_E^I]\left(F_{imp}\boldsymbol{n}\right). \quad (36)$$

Based on Eq. (36), a new internal impulse measure that quantifies the ability to withstand external impulse at joints is defined by

$$w_{ii} = \sqrt{\det\{[S_E^I]^T[S_E^I]\}}, \quad (37)$$

and the measure w_{ii} can be found as

$$w_{ii} = \bar{\sigma}_1\bar{\sigma}_2\cdots\bar{\sigma}_n, \quad (38)$$

where $(\bar{\sigma}_1, \bar{\sigma}_2, \cdots \bar{\sigma}_n)$ are the square roots of the singular values of $[S_E^I]^T[S_E^I]$. The singular value means relative magnitudes of the internal impulse corresponding to the unit ball of changes in the external impulse.

VII. Simulation

Human sawing task is modeled based on the parameters of male adults [7]. The numerical values of the kinematic and dynamic parameters used in simulation are presented in Table 1. Fig. 7 (a) and (b) represent the models of human sawing task using one arm and two arms (i.e., dual-arm), respectively. Human sawing task using one arm is modeled as a 3-linked planar serial manipulator. θ_1, θ_2, and θ_3 represent the shoulder joint, the elbow joint, and the wrist joint of the human arm, respectively. And the third link represents the human hand grasping the sawing tool. In a similar manner, human sawing task using a dual-arm is modeled like Fig. 7 (b). The purpose of sawing task will be to maximize the external impulse exerted on the object to be sawn by the saw and to minimize the internal impulse experienced at the joints of the human upper-extremity.

The velocity of the moving saw is given 0.6 m/s to the right direction. Coefficient of restitution e is assumed zero because of the plastic deformation of the object being sawed. The test workspace is a rectangular region having $0.35 \le x \le 0.65$ (m) and $-0.4 \le y \le 0.4$ (m), as displayed in Fig. 7.

The characteristics of the external impulse and the internal

impulse can be observed in terms of the impulse geometry. Fig. 8 and Fig. 9 denote the impulse geometries described by normalized impact geometry [8]. The dashed line denotes the external impulse and the solid lines represent the internal impulse at the joints. We have following conclusion. First, the area of the external ellipsoid for the dual arm is shown larger than that of the single arm by comparison of Fig. 8(a) and Fig. 8(b) and comparison of Fig. 9(a) to Fig. 9(b), respectively. This implies that the dual arm is superior to the single arm in aspect of external impulse. Second, the internal impulses of the single arm and the dual arm are almost identical for the same task while the external impulse of the single arm is less than that of the dual arm by comparison of Fig. 8(a) and Fig. 8(b) and comparison of Fig. 9(a) and Fig. 9(b), respectively. However, in order for the serial arm to create the same amount of the external impulse experienced at the dual arm, Fig. 8(c) and Fig. 9(c) show that the amount of the internal impulse of the single arm gets larger than that of the dual arm given in Fig. 8(b) and Fig. 9(b). Through more detailed analysis over the whole workspace, an optimal sawing region can be identified in which the amount of external impulse is maximized and the amount of the internal impulse is minimized. The workspace along the x direction with the value of y around -0.3m is found the optimal sawing region. This result is coincident to the human experience.

In addition to the known advantages of dual or multiple cooperating arms over one single arm, the above analysis shows that the dual arm has another advantage in aspect of external impulse and internal impulses.

VIII. Conclusion

It has been reported that the dual-arm has many advantages over the single arm. In this work, we demonstrate another merit of using the dual-arm in aspect of external/internal impulse through a human sawing task. General conclusion is that the external/internal impulse exerted on objects and joints largely depends on the geometry and dynamic characteristics of manufacturing tasks. Specifically, utilization of dual arm or multiple arms is effective to enhance the performance of the sawing task in aspect of maximizing external impulse and minimizing internal impulse of the joints.

References

[1] I.D. Walker, "Impact configurations and measures for kinematically redundant and multiple armed robot systems," *IEEE Transactions on Robotics and Automation*, Vol. 10, No. 5, pp. 670-683, 1994.

[2] H.-T. Liao and M. C. Leu, "Analysis of impact in robotic peg-in-hole assembly", *Robotica*, Vol. 16, No. 3, pp. 347-356, 1998.

[3] Y.-F. Zheng and H. Hemami, "Mathematical modeling of a robot collision with its environment," *Journal of Robotic Systems*, Vol. 2, No. 3, pp. 289-307, 1985.

[4] J. Wittenburg, *Dynamics of systems of rigid bodies*, B.G. Teubner, Stuttgart, 1977.

[5] H. J. Kang, B-J. Yi, W. Cho, and R. A. Freeman, "Constraint-embedding approaches for general closed-chain system dynamic in terms of a minimum set," Proc. Of 1990 ASME Biennial Mechanism Conference, Chicago, IL, DE-Vol. 24, pp. 125-132, 1990.

[6] R. M. Brach, "Classical planar impact theory and the tip impact of a slender rod," *International Journal of Impact Engineering*, Vol. 13, No. 1, pp. 21-33, 1993.

[7] D.B. Chaffin, B.J. Gunnar, and Anderson, "Occupational Biomechanics," A Willey-Interscience Publication, John Wiley & Sons, 1984.

[8] J. Kim, W.K. Chung, and Y. Youm, "Normalized Impact Geometry and Performance Index for Redundant Manipulators," Proc. of the 2000 IEEE Int. Conference on Robotics and Automation, pp. 1714-1719, 2000.

[9] S.H. Lee, B.-J. Yi, S.H. Kim, and Y.K. Kwak, "Modeling and Analysis of Internal Impact for General Classes of Robotic Mechanism," Proc. of IEEE /RSJ Int. Conference on Robots and Intelligent Systems, pp. 1955-1962, 2000.

[10] G. Ferretti, G. Magnani, and A. Zavala Rio, "Impact modeling and control for industrial manipulators," IEEE Control System Magazine, Vol. 18, No. 4, pp. 65-71, 1998.

[11] J. K. Mills and C. V. Nguyen, "Robotic manipulator collisions: Modeling and simulation," ASME Journal of Dynamic Systems, Measurement, and Control, Vol. 114, No. 4, pp. 650-659, 1992.

[12] K. Youcef-Toumi and D. A. Gutz, "Impact and force control," Proc. of IEEE Int. Conference on Robotics and Automation, pp. 410-416, 1989.

Table 1. Kinematic/Dynamic Parmeters of Human Arm Model

	Length(m)	Mass(kg)	Inertia(x,y,z ; $kg \cdot m^2$)
l_1	0.33	2.10	(0.0035,0.0208,0.0208)
l_2	0.26	1.274	(0.00136,0.00786, 0.00786)
l_3	0.5	1.70	(0.00056,0.0359,0.0355)
l_4	0.33	2.10	(0.0035,0.0208,0.0208)
l_5	0.26	1.274	(0.00136,0.00786, 0.00786)
l_b	1.0	-	-

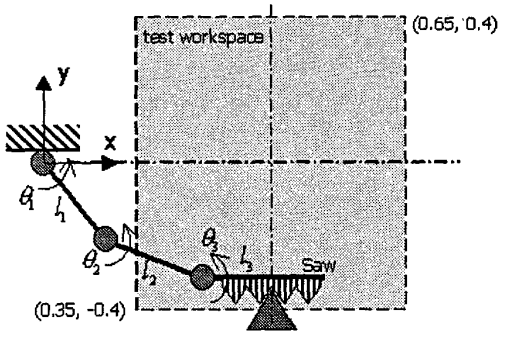

(a) Single Arm Model

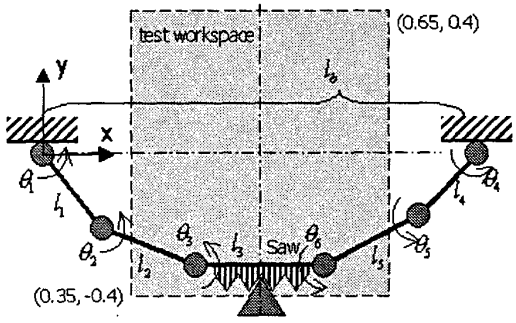

(b) Dual Arm Model

Fig. 7. Models of Human Sawing Task

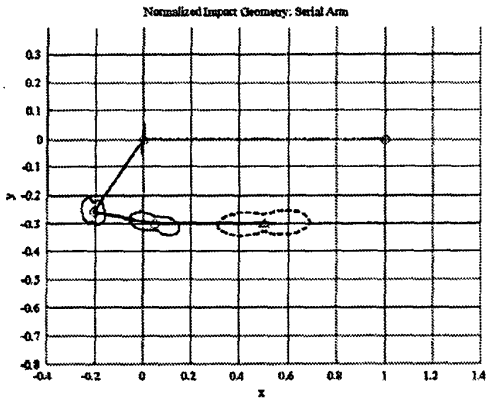

(a) Single Arm

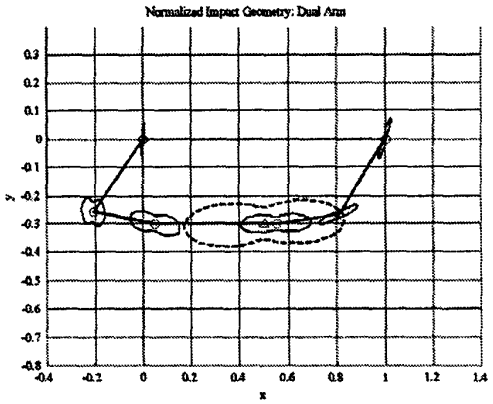

(b) Dual Arm

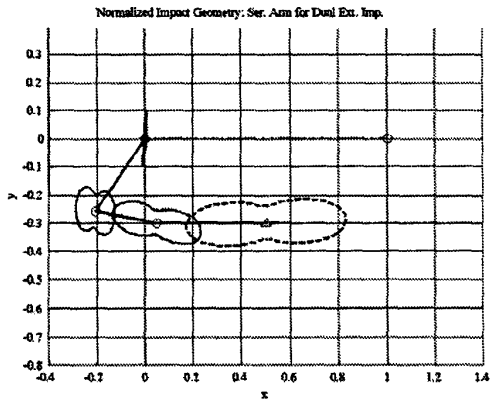

(c) Single Arm with External Impulse of Dual Arm
○ : joint, △ : contact point
solid line: internal impulse ellipse
dashed line : normalized external impulse ellipse

Fig. 8. Geometries of Normalized Internal and External Impulses at (x, y)=(0.3, -0.3)

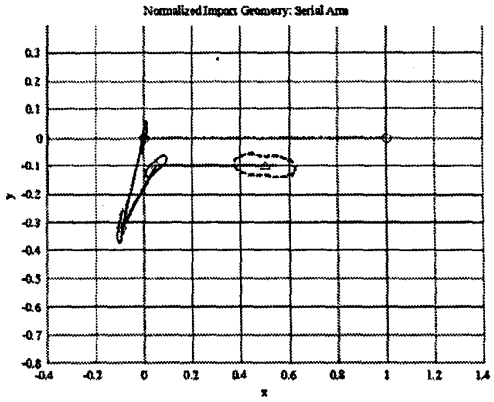

(a) Single Arm

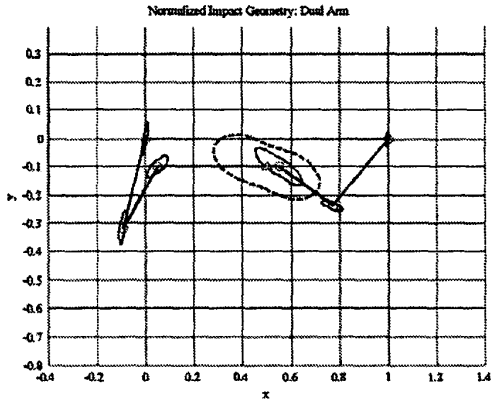

(b) Dual Arm

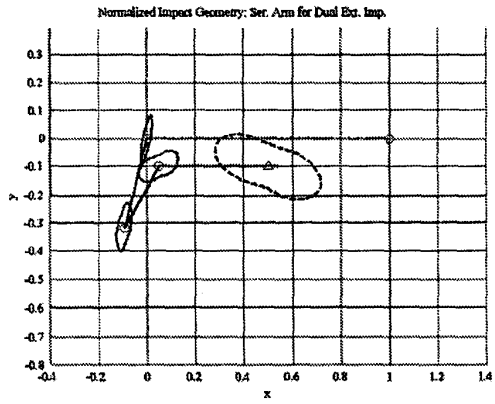

(c) Single Arm with External Impulse of Dual Arm
○ : joint, △ : contact point
solid line: internal impulse ellipse
dashed line : normalized external impulse ellipse

Fig. 9. Geometries of Normalized Internal and External Impulses at (x, y)=(0.3, -0.1)